Journal of Alloys and Compounds 765 (2018) 1018–1025

Contents lists available at ScienceDirect

Journal of Alloys and Compounds

journal homepage: http://www.elsevier.com/locate/jalcom

The effect of surface roughness of the substrate on fatigue life of coated aluminum alloy by micro-arc oxidation

Wei Bing Dai [a], Long Xiang Yuan [a], Chang You Li [a, *], David He [a, **], Da Wei Jia [b], Yi Min Zhang [c]

[a] School of Mechanical Engineering and Automation, Northeastern University, Shenyang, China
[b] AVIC SAC Commercial Aircraft Co., Ltd., Shenyang, China
[c] School of Institute of Equipment Reliability, Shenyang University of Chemical Technology, Shenyang, China

ARTICLE INFO

Article history:
Received 20 April 2018
Received in revised form
22 June 2018
Accepted 24 June 2018
Available online 26 June 2018

Keywords:
Surface roughness
Fatigue life
Micro-arc oxidation
Interface
High cycle fatigue
High alternating stress

ABSTRACT

In the present work, ceramic coatings are deposited on the surface of 2024-T3 aluminum (Al) alloy by micro-arc oxidation (MAO). The Surface roughness of the Al alloy substrate is different in the range from 0.2 μm to 1.6 μm. This paper investigates the effect of surface roughness of the Al alloy substrate and surface treatment on the fatigue properties of 2024-T3 Al alloy. The morphology, microstructure, and phase composition of the oxide layers are examined using X-ray diffraction (XRD) and scanning electron microscopy (SEM). Surface roughness of the coatings was measured using a 3D measuring laser microscope. The fatigue life of the Al alloy is evaluated under high and low cyclic stress. The results of the investigation have shown that the fatigue life of the coated samples with Ra = 0.2 μm is higher than others. The fatigue life of coated samples with Ra = 0.8 μm is very close to that with Ra = 1.6 μm under high cycle fatigue conditions. The reason is that the roughness of the interface between substrate and coating affects the fatigue life of coated samples. In contrast, the fatigue property changes when the coated samples were applied to high alternating stress. The fatigue performance of the coated Al alloy with Ra = 0.8 μm is the worst, followed with Ra = 1.6 μm. The rougher surface and the concentrating distribution of hills and valleys lead to this result.

1. Introduction

Aluminum (Al) alloy, with high strength and low specific gravity, is the preferred material in automotive and aerospace industries [1,2]. However, the wear resistance and corrosion resistance of Al alloy are poor. The two disadvantages restrict its extensive applications [3–5]. Micro-arc oxidation (MAO) technique is a cleaning process and a new surface modification technology of ceramic oxide film on the surface of nonferrous metal [6]. And the coatings are combined well with the substrate [5,7,8]. The coated samples, with hard, thick, and dense ceramic coatings, showed ideal performance of excellent wear and high corrosion resistance [9–11]. While the coatings improve the surface properties of the Al alloy, the oxidation treatment has an adverse effect on the fatigue life of the substrate [12–16]. Yerokhin et al. [12] showed thicker coatings reduce the fatigue properties of the Mg alloy treated by MAO. Strain distortion of Mg subsurface layers introduced by coatings is the main reason. Furthermore, Kong et al. [14] concluded that the overgrowth region of MAO coating into substrate is an important reason for the decline in fatigue limit. The locations of the overgrowth easily produce stress concentration and induce the formation of fatigue crack. In addition, residual tensile stress introduced by the coating on the substrate surface promotes crack initiation. At high cycle fatigue conditions, Lonyuk et al. [15] and his co-workers studied the cause of the decline in fatigue life of 7475-T6 with MAO coating. The conclusions are similar to the results by Kong. And this paper also clearly pointed out the fatigue crack initiation was in the substrate adjacent to the coating. The residual compressive stress within the coating has some benefits on fatigue life compared to hard oxidation. Wang et al. [16] calculated in theory the value of the reduction factor for the fatigue strength of the overgrowth zone near the interface. The decline of fatigue life was caused by the notch sites. However, Leoni et al. [13] believed that the micro-cracks, micro-pores, and surface roughness of the

* Corresponding author.
** Corresponding author.
E-mail addresses: chyli@mail.neu.edu.cn (C.Y. Li), davidhe@uic.edu (D. He).

https://doi.org/10.1016/j.jallcom.2018.06.290
0925-8388/

coating surface affect the fatigue life of coated material in addition to notch sites. These results will provide support for further study of the fatigue life of micro-arc oxidation. Moreover, by studying the reason of the decrease of the fatigue life of micro-arc oxidation, pretreatment of the substrate before micro-arc oxidation can reduce the adverse effect [17,18]. Thus the MAO technology will have a very wide range of applications in the aviation industry [6]. Asquith et al. [17] employed shot peening to make the surface of the substrate introduce residual compressive stress. Wen et al. [18] adopted nanocrystalline layer to make the surface of the substrate residual compressive stress. Residual compressive stress improved the fatigue properties of the coated material by MAO. Wang et al. [19] applied sealing pore technology to improve the fatigue property of the coated samples by MAO. The reason is that the epoxy resin welded the thermal cracks and filled micro-pores of the coatings. In sum, it is significant to carry out the research of MAO in practical application.

At present, the research of MAO process mostly grinds the substrate to a lower surface roughness [15,20,21], but increases the pretreatment work and the cost. In the manufacturing process, the material grinding does not conform to the actual production conditions. Thus it is of great significance to study the influence of surface roughness of the substrate on the coated samples. To date, there is no report on the fatigue behavior of 2024-T3 aluminum alloy subjected to MAO process with different surface roughness of the substrate. The paper investigates the effect of surface roughness on the fatigue performance of an Al2024 alloy.

2. Experimental details

2.1. Coating preparation

12. A heat-treated plate of Al 2024 alloy (Cu 3.8–4.9%, Si 0.5%, Fe 0.5%, Mn 0.3–0.9%, Mg 1.2–1.8%, Zn 0.25%, Cr 0.1%, Ti 0.15%, Al the rest) with 1.6 mm in thickness was used as substrate for MAO coating. The T3 heat treating condition consists of a solution heat treatment, cold working, and natural aging [22]. The samples used for axial tensile–tensile fatigue testing were cut from parent plate using wire cutting machine. The specimen geometry is given in Fig. 1. The results of static tension carried on 2024-T3 aluminum alloy are $\sigma_b = 466$ MPa (ultimate tensile strength), $\sigma_{0.2} = 333$ MPa (yield strength), and $\delta = 22.8\%$. Then test specimens having an initial roughness of Ra = 0.8 μm were polished to the roughness of Ra = 0.2 μm and Ra = 1.6 μm, respectively.

Prior to MAO treatment, the substrates of Al alloy were degreased with alcohol and rinsed with water. The number of specimens for each surface roughness is set to 15. All Al alloy specimens were bolted to a copper plate mounted on the anode of the electrolytic bath (Fig. 2). The MAO equipment used stainless steel as a counter electrode. The samples were immersed in an alkaline silicate solution containing Na_2SiO_3 (6.0 g/L), NaOH (1.2 g/L), $(NaPO_3)_6$ (35.0 g/L), and Na_2WO_4 (6.0 g/L) in distilled water. This can reduce the error caused by changes in the experimental

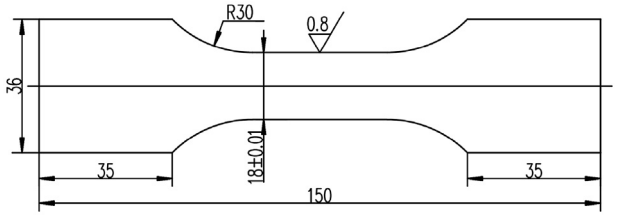

Fig. 1. Dimension of 2024-T3 alloy used in fatigue testing.

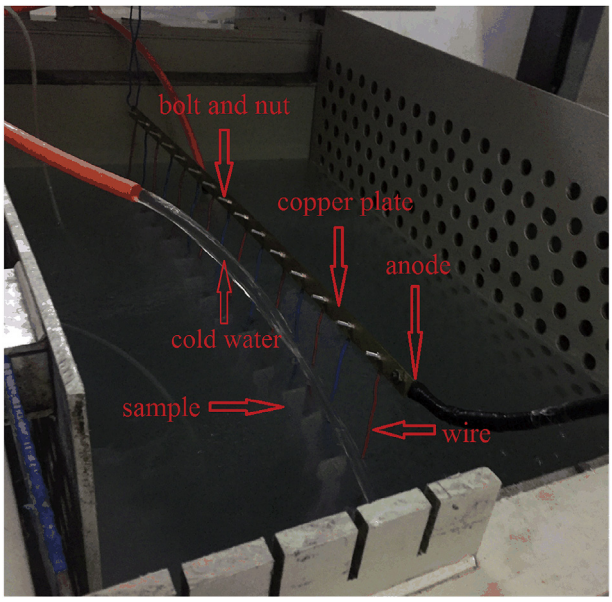

Fig. 2. Test piece and the anode connection.

environment. It should be noted that the material of the bolt and nut used for the connection is aluminum alloy. The MAO treatment was carried out under constant voltage of 500 V, with a duty cycle of 10%, and frequency of 600 Hz for 12 min. A 65 kW MAO device is adopted to offer energy [16]. Sample codes are given in Table 1. In Fig. 2, it can be seen that cold water was injected to the electrolyte bath. So the electrolyte temperature could be controlled to remain lower than 50 °C. After the MAO treatment, the specimens were removed from the electrolyte, washed with water, and dried with a blower.

2.2. Coating characterization

The thickness of coatings was determined using the eddy current thickness gauge (GTS810NF, GUOOU) at ten randomly selected locations, and thickness was calculated by the average of the measurements. The field emission scanning electron microscopy (SEM, Ultra Plus, Carl Zeiss AG) was employed to examine the microstructure and the cross-section morphology of the oxide layers. The crystallographic characteristics of the oxides were investigated using X-ray diffraction (XRD, Cu-Kα, 40 KV-40 mA, Philips, Netherlands) over 2θ range from 20° to 80° at a scan rate of 1.5°/min. The surface roughness (Ra) of coatings was measured using a 3D measuring laser microscope (LEXT OLS4100). Average values were calculated as the surface roughness.

2.3. Fatigue studies

The mechanical behavior of bare 2024-T3 Al and MAO coated fatigue samples were evaluated using a PC controlled EHF-EV200K2-040-1A machine. The experimentations including static tension and fatigue tests were done. The influence of the MAO coating on the mechanical properties of the substrate is studied in this paper. All samples were subjected to axial tensile–tensile fatigue test at 20 Hz frequency with a sinusoidal cycle of a stress ratio (minimum load to maximum load) of 0.1. The fatigue property is evaluated under low (390 MPa and 350 MPa) and high cycle (240 MPa and 220 MPa) fatigue conditions. Thus the fatigue life of the coatings formed on substrate with Ra = 0.2 μm and Ra = 1.6 μm is discussed compared to Ra = 0.8 μm. For the sake of more accurate

Table 1
Different process parameters used during the experiment for each sample.

Sample codes	Applied voltage (V)	Surface roughness of substrate Ra (μm)	Duration time (minutes)
a	500	0.2	12
b	500	0.8	12
c	500	1.6	12

values, three coated specimens were tested at one stress level, and the average fatigue life was obtained.

3. Results and discussion

3.1. Microstructure of coating

The surface roughness and coating thickness of coatings formed on the 2024-T3 Al with different roughness of substrate are presented in Table 2. The calculation result of coating thickness is 5.1 μm, 4.6 μm, and 4.7 μm for coatings a, b and c, respectively. It shows that the roughness of the substrate has less effect on the coating thickness in 12 min of surface treatment. The roughness values are 0.40 μm, 0.69 μm and 0.74 μm for coatings a, b and c, respectively. The surface roughness of the coatings is lower than that of substrate except for the roughness of Ra = 0.2 μm. The oxide layers, with pores and pancake projections, made the surface of smooth substrate rough [21]. However, the defect of a rough surface was covered by the coatings. Consequently, the surface roughness of coated samples was improved. Fig. 3 shows that the three dimensional surface profiles of the coated samples. It can be seen that the distribution of hills and valleys is relatively concentrated on its surface as shown in Fig. 3b compared to other coatings. This will promote crack propagation. In addition, the surface profile shows that the roughness of the sample a and b is lower compared to that of sample c. The surface of the specimen c has shallow grooves, which are caused by grinding the specimen before MAO treatment. In fact, the direction of these grooves is not perpendicular to the tensile stress applying to the specimen. Therefore, MAO treatment has less effect on the mechanical properties of the material.

The surface morphologies of coatings were examined using SEM and SEM micrographs are shown in Fig. 4. Images of d, e, and f are the enlarged that of a, b, and c, respectively.

The SEM micrograph shows that a larger number of smaller pores distributed all over the surfaces as shown in Fig. 4, but the surface of the coating for sample a has some pores with 2–3 μm in diameter. However, for sample b, the size in diameter of many pores is less 2 μm (Fig. 4e) and very few are 3–4 μm (Fig. 4b). The diameter of most micro-pores on the surface of specimen c is 1 μm. The relatively large size of the pores can accelerate the growth of the coating [23]. Thus the coating of the specimen a is thicker. Moreover, research has shown that the molten metals extruded from the discharge channel and they are rapidly cooled to form oxides that adhere to the substrate when encountering the electrolyte [24]. Therefore, the surface of the coating has a volcanic spray-like surface topography. Under the high voltage, the position of the thinner coating is easy to be punctured to form the discharge channel [24–26]. Due to the same pulse duty cycle, the large energy input leads to larger pores on the coating with less discharge channel [26,27]. So the coating surface of sample a has large size pores. The coating surface of sample b and c has many small pores and the coating is also not evenly distributed. This can also be seen in Fig. 3. However, pores are likely to become crack initiation sites.

Table 2
Coating thicknesses and surface roughness of coated samples.

Sample	Average coating thickness (μm)	Surface roughness, Ra (μm)
a	5.1	0.40
b	4.6	0.69
c	4.7	0.74

The cross-section of the sample formed under the conditions described in Table 1 shows two regions distinguished by color and density (Fig. 5). In particular, the oval markings in Fig. 5b are the result of polishing during specimen preparation and the films are not separated from the substrates [27]. It should be pointed that the interface between substrate and oxidation film is inclined to be rather zigzag as shown in Fig. 5b and c, which is not the overgrowth sites, but rather caused by the rough surface of the substrate. And the interface for the roughness of Ra = 0.2 μm shown in Fig. 5a is smooth. The investigation has shown that the notch of the interface is prone to be areas of stress concentration and crack initiation [16].

Fig. 6 shows XRD patterns of MAO coated samples a, b, and c, which were prepared using different process parameters listed in Table 1. It can be seen that the diffraction peaks of Al 2024 alloy are strongly detected. Because the coatings are thin and have lots of micro-pores on the surface and the X-rays can easily penetrate through it [14]. In order to observe other diffraction peaks, the diffraction peaks of Al alloy are taken as a part. Thus as shown in Fig. 6, the coatings for different roughness of substrate mainly consist of γ-Al_2O_3 phase and a small amount of α-Al_2O_3. In the initial stage of MAO, there are many discharge channels on the surface of the coating, which promote the electrolyte entering the substrate. Thus the electrolyte encounters with the molten alumina that ejected out from the channel and encourages the formation of γ-Al_2O_3 phase during solidification of alumina droplets [23,24].

It has been reported that γ-Al_2O_3 phase in the coatings can generate residual compressive stress on the surface of substrate and inhibit the initiation and propagation of cracks [15,17].

3.2. Fatigue studies of coated samples

Fig. 7 shows the fatigue life date for the substrate (Ra = 0.2 μm) and the coated specimens at σ_{max} = 220 MPa, σ_{max} = 240 MPa, σ_{max} = 350 MPa, and σ_{max} = 390 MPa. The surface roughness of 2024-T3 plate applied to the aircraft structure is Ra = 0.8 μm. It can be seen that the fatigue life of the sample a is increasing compared to corresponding that of the substrate at four stress levels. On the one hand, the substrate near the interface between substrate and coating is subjected to compressive stress. The compressive stress is caused by the different coefficients of thermal expansion of the substrate and the coating (α_{Al} (~24×10^{-6}/°C)>$\alpha_{\gamma\text{-}Al2O3}$(~$6.2 \times 10^{-6}$/°C)) [28]. Wasekar et al. [29] tested the residual stress of the 15 μm thick coating (mainly γ-Al_2O_3 phase) and found that the γ-Al_2O_3 produced a compressive stress of 126 MPa on the substrate. And the compressive stress can inhibit the initiation and propagation of cracks [15,25,30]. On the other hand, the surface roughness of the sample becomes lower after micro-arc oxidation (Table 2), which helps to improve the fatigue performance. However, the effect of the coating on the fatigue life of the substrate is not significant for sample b. Under the low cycle fatigue conditions, the crack

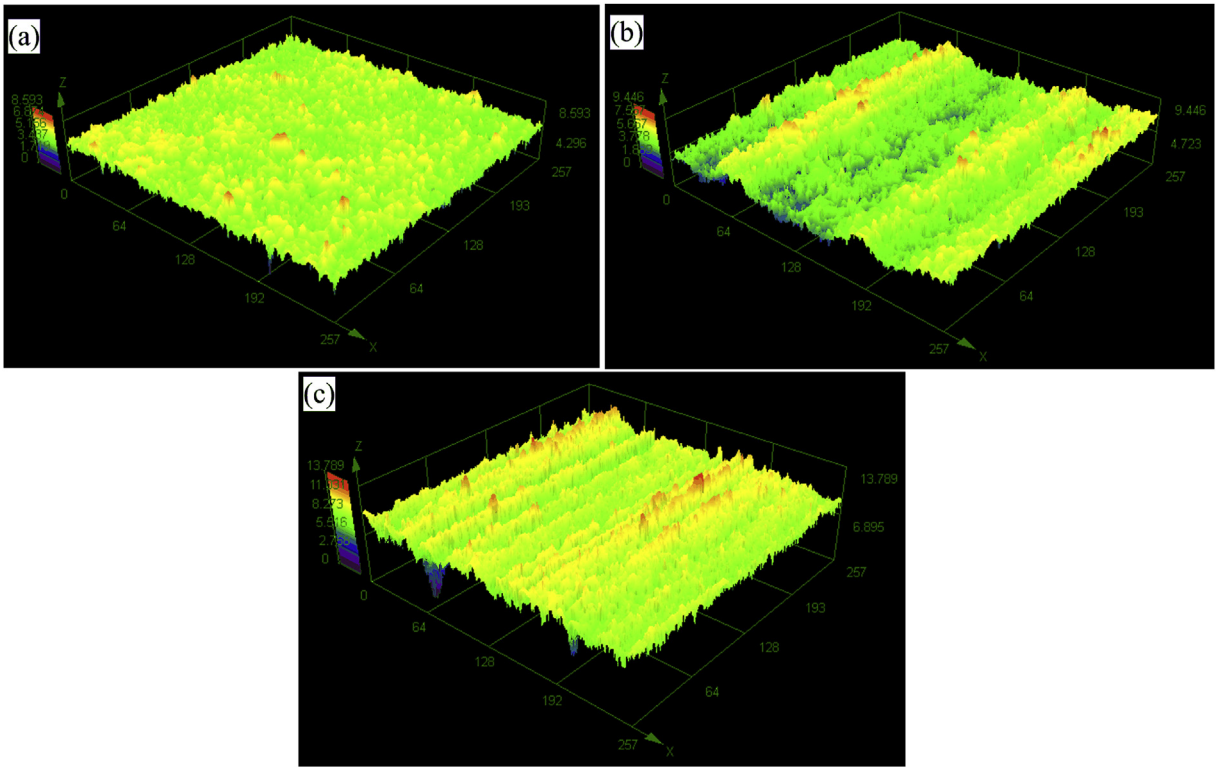

Fig. 3. 3D surface profiles of the oxides obtained by MAO carried out under the conditions described in Table 1 for (a) Process a, (b) Process b, (c) Process c.

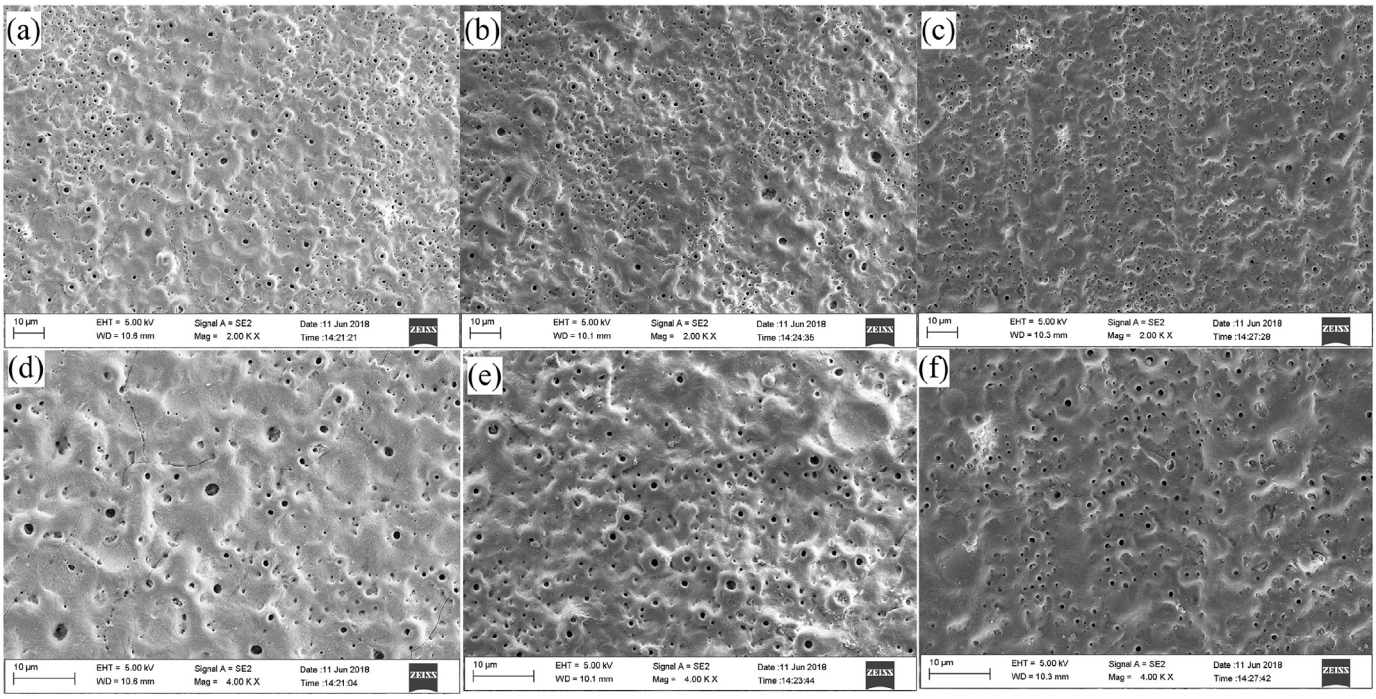

Fig. 4. Surface morphologies of the oxides obtained by MAO carried out under the conditions described in Table 1 for (a) (d) Process a, (b) (e) Process b, (c) (f) Process c.

propagation life is the main part of the fatigue failure [31]. According to the 3D surface profiles of sample b, the concentrating distribution of hills and valleys promotes crack propagation and weakened the fatigue properties of the coated specimen. When the low alternating stress is applied, the crack propagation period is relatively small, and the crack initiation period is the major part. Therefore, under the high cycle fatigue conditions, the fatigue life of the sample b is clearly better than that of the substrate.

In order to explain the effect of the change of surface roughness on the fatigue life of coated specimen treated by MAO, the variable

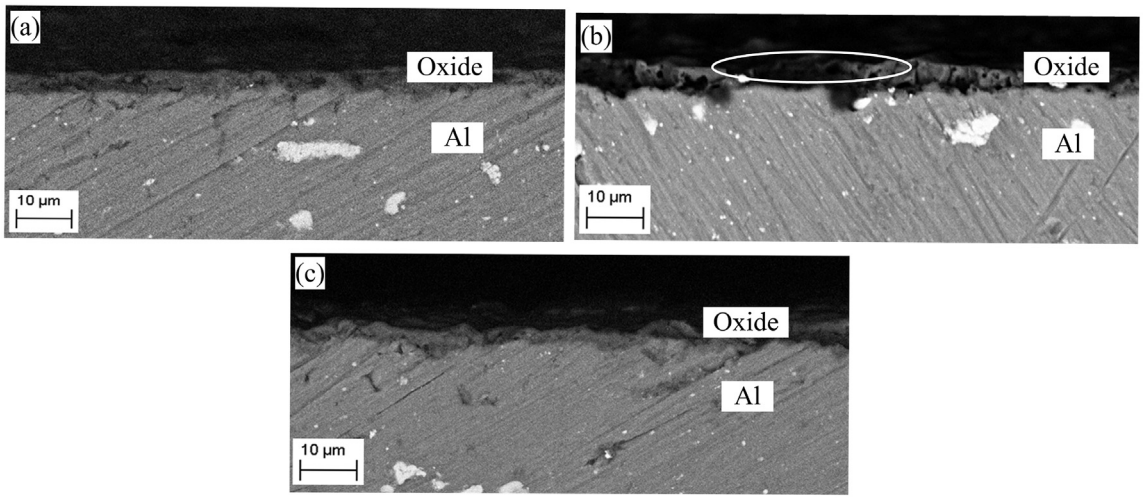

Fig. 5. Cross-sectional view of the oxide layers obtained by MAO carried out under the conditions described in Table 2 for (a) Process a, (b) Process b, (c) Process c.

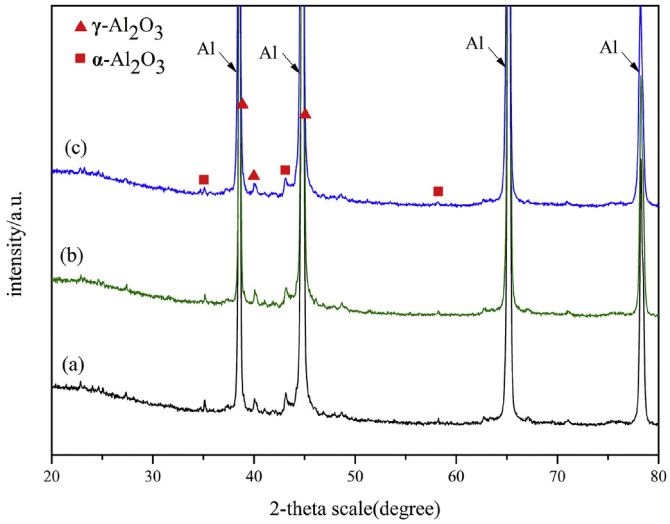

Fig. 6. XRD pattern of the oxide layers under the conditions described in Table 1 for (a) Process a, (b) Process b, (c) Process c, with the respective phases identified.

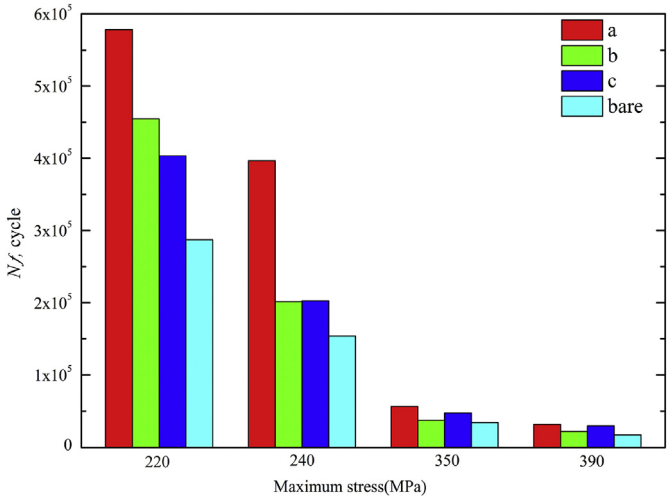

Fig. 7. Fatigue life of bare specimens (Ra = 0.8 μm) and coated specimens oxidized under the conditions described in Table 1 for (a) Process a, (b) Process b, (c) Process c.

η is defined as:

$$\eta = N_f' / N_f \quad (1)$$

where N_f' is fatigue life of the sample a and c, N_f is fatigue life of the sample b. The values are listed in Table 3. According to the data η in Table 3, it is easy to find that the fatigue life of the specimen a is higher than that of the others in both high and low cycle fatigue conditions. For the simple c, its fatigue life is higher than that of sample b at $\sigma_{max} = 350$ MPa and $\sigma_{max} = 390$ MPa. However, compared with the sample b at $\sigma_{max} = 220$ MPa and $\sigma_{max} = 240$ MPa, the fatigue performance of the sample c is relatively poor. Li et al. [32] studied the effect of different surface roughness on the fatigue life of medium carbon steels. It is concluded that the influence of surface roughness (Ra = 0.4 μm, Ra = 0.8 μm and Ra = 1.6 μm) is not significant under the high cycle fatigue conditions. When low alternating stress is applied, as the surface roughness increases, the fatigue life decreases gradually and the mean of the fatigue life with Ra = 0.8 μm is very close to that with Ra = 1.6 μm. From the cross-sectional view of the oxide layers in Fig. 5, thinner coatings do not introduce defects into the substrate surface, which is similar to [33].

And the interface between substrate and coating plays an important impact on fatigue life [14,16]. The roughness of interface for sample a, b and c is Ra = 0.2 μm, Ra = 0.8 μm and Ra = 1.6 μm. When low alternating stress is applied, the result of the fatigue life (Table 3) at $\sigma_{max} = 220$ MPa and $\sigma_{max} = 240$ MPa coincide well with

Table 3
The fatigue life of the sample a and c (N_f') and the sample b (N_f) and the value of η

σ_{max}	sample	N_f'	N_f	η
220 MPa	a	578140	–	1.271
	b	–	454832	–
	c	403415	–	0.887
240 MPa	a	396398	–	1.966
	b	–	201584	–
	c	202800	–	1.006
350 MPa	a	56381		1.516
	b	–	37190	–
	c	47433		1.275
390 MPa	a	31532	–	1.436
	b	–	21960	–
	c	29663	–	1.351

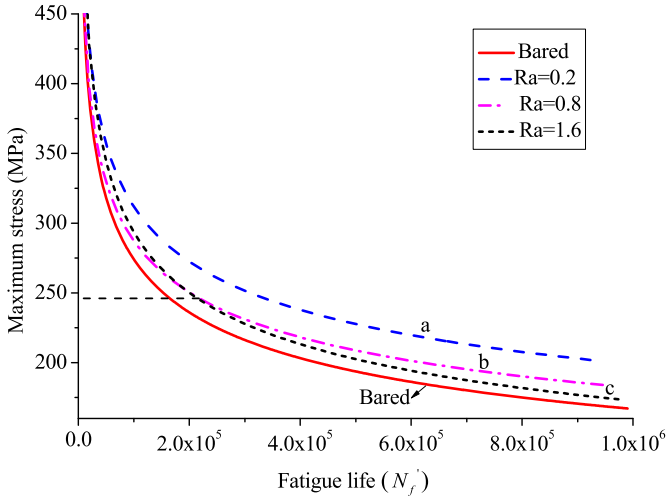

Fig. 8. The S-N curves of samples a, b, c, and bare Al alloy (Ra = 0.8 μm).

results by Li and his coworker. Under the low cycle fatigue conditions, the surface roughness of the coating affects the fatigue life of the coated specimen [25]. The samples with smoother surface roughness of coating have excellent fatigue property. So the fatigue life of sample a is higher than that of the others. However, the distribution of valleys for sample b distributes is relatively concentrated. Thus the crack is spread very fast from the surface of coating to the interface between the coating and the substrate. The reason why the fatigue life of the sample c is higher than that of the sample b is that the existence of the groove hinders the propagation speed of the crack.

Table 4
Material constant of coated samples by MAO with different roughness of substrate and bare Al alloy.

Sample	k	C_S
a	5.110	5.56×10^{17}
b	5.038	2.43×10^{17}
c	4.338	5.07×10^{15}
Bared	4.634	1.98×10^{16}

Fig. 8 shows the S-N curves for sample a, b, c, and bare Al alloy. The least squares method is used to fit the fatigue test data to obtain the material constants k and C_S. The values are shown in Table 4. The resulting material constants are brought into the Basquin equation (Equation (2)) to obtain the S-N curve [34].

$$S_{\max}^{k} N_f' = C_S \tag{2}$$

$S_{\max}$ is maximum stress.

The curves of specimen a at the stress level of 150 MPa–450 MPa are all above the curves of others, and the fatigue performance is the best. The curve of bare aluminum is the

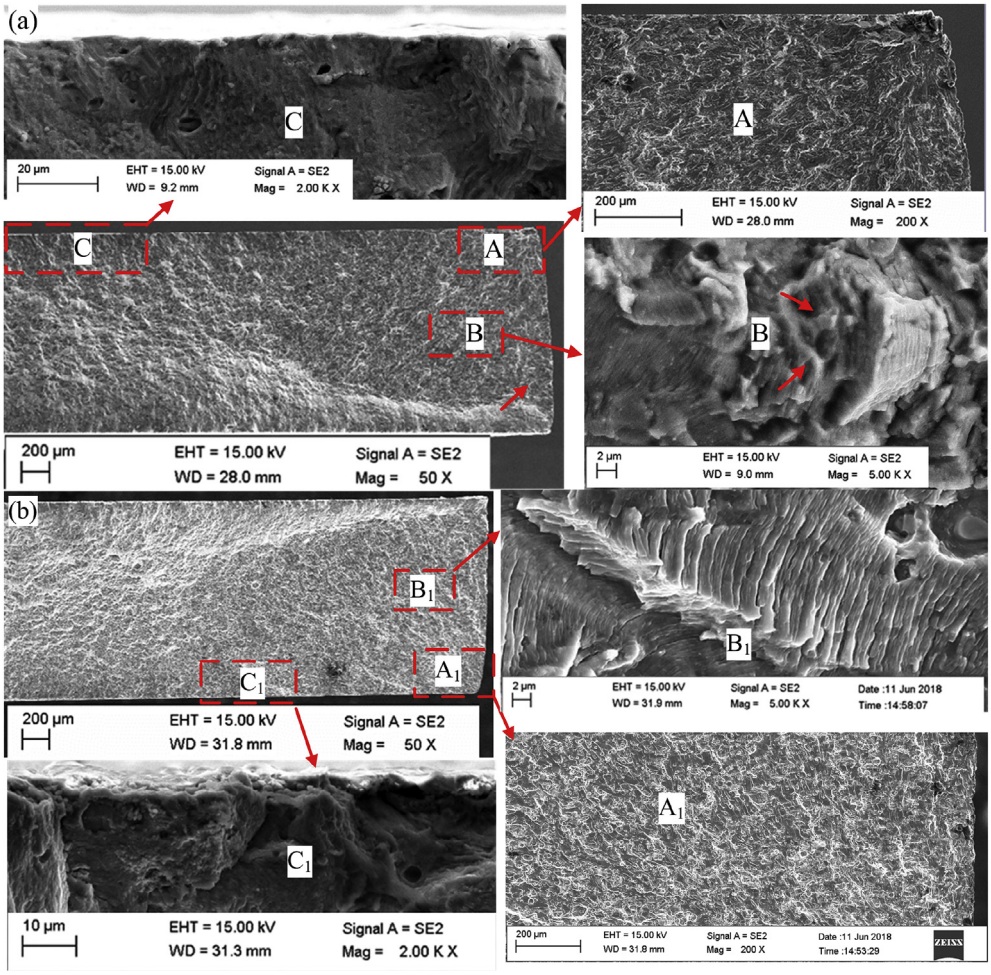

Fig. 9. The fatigue fractural surface morphology of (a) bare Al (Ra = 0.8 μm) alloy, (b) sample b.

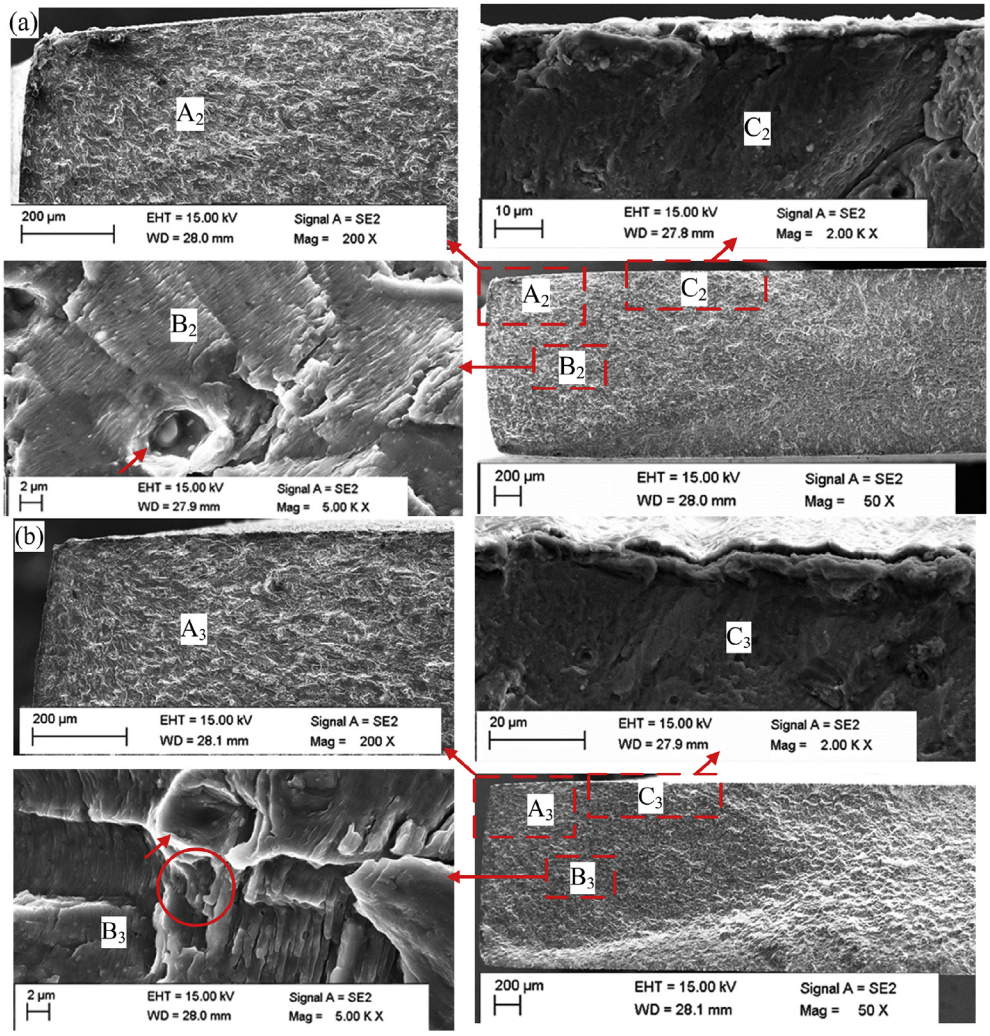

Fig. 10. The fatigue fractural surface morphology of (a) sample a, (b) sample c.

opposite, and the fatigue life is the worst. However, the curves of specimens b and c have intersections at $S_{max} = 240$ MPa. As discussed earlier, the fatigue performance of sample b and c is different in the stress range of 150 MPa–240 MPa and 240 MPa–450 MPa.

Before and after the micro-arc oxidation, the fatigue fracture morphologies of Al alloy are shown in Fig. 9. Fatigue lines exist in fatigue fractures. It can be seen that the zones of crack initiation marked as A and A_1 are on the surface of the sample. Stress concentration and surface defects may be the causes of crack initiation. Crack propagation zone of coated and uncoated sample is different as shown B and B_1. Although they all have fatigue stripes, there are brittle fatigue stripes in zone B, as indicated by the arrows. The number of fatigue stripes represents the number of cyclic loads applied. Thus the crack propagation life of bare Al alloy becomes shorter because of the presence of brittle fatigue stripes. And differences in the internal microstructure of the Al alloy cause the fatigue stripes not in one plane and direction. The zones marked C and C_1 are the morphologies of the surface of samples. The coated sample has a rougher fracture surface than the bare Al alloy. This is caused by the microscopic defects of the coating.

Fig. 10 shows that the fracture morphologies of sample a and sample c. It can be seen that the zones of crack initiation marked A_2 and A_3 are same as the bare Al and sample b. Moreover, all the samples in Figs. 9 and 10 marked B, B_1, B_2, and B_3 have second cracks, but sample a has less second cracks. Therefore, the morphology of fatigue stripes marked B_2 for sample a are smoother than that of fatigue strips for other samples. The pit may be caused by the presence of inclusions inside the Al alloy for crack propagation zone pointed by the arrow in Fig. 10. However, the circular marking area is the brittle part of the sample c. Under high-cycle fatigue conditions, this is a factor that affects the fatigue life. It is worth noting that the fracture surface of the specimens a and c is flatter than that of the specimen b. This is due to multiple cracks on the coating surface of sample b.

4. Conclusions

All of coatings formed on the substrate with different surface roughness mainly consist of γ-Al_2O_3 and small amounts of α-Al_2O_3. And the substrate near the interface between substrate and coating is subjected to residual compressive stress due to the existence of γ-Al_2O_3. The residual compressive stress can improve the fatigue performance of the specimen. Moreover, thinner coatings do not introduce defects into the substrate surface. After MAO treatment, the surface of the coatings for the substrate with Ra = 0.2 μm become rougher, while that for the substrate with Ra = 0.8 μm and Ra = 1.6 μm become smoother. Especially, the distribution of hills and valleys is relatively concentrated on its surface for the sample with Ra = 0.8 μm.

Under the high cyclic stress of 350 MPa and 390 MPa, the effect of surface roughness of the coating on the fatigue life of the coated specimens is significant. The rougher the surface of coating is, the lower the fatigue life is. However, the concentrating distribution of hills and valleys is harmful to the fatigue life. For the high cycle fatigue life, roughness of the interface between substrate and coating plays an important impact on fatigue life. As the surface roughness of the interface decreases, the fatigue life increases.

This paper offers new insights into the effect of the surface roughness of the substrate on the fatigue life of coated samples. It is expected that the results of the paper could be utilized to promote the application of the MAO technology in production practice and reduce production cost.

Acknowledgments

The work is supported by National Natural Science Foundation of China (grant Nos. 51575095, 51675089, U1708254), and China Postdoctoral Science Foundation (2017M610180).

References

[1] E.A.S. Jr, J.T. Staley, Application of modern aluminum alloys to aircraft, Prog. Aero. Sci. 32 (1996) 131–172.
[2] A. Heinz, A. Haszler, C. Keidel, S. Moldenhauer, R. Benedictus, W.S. Miller, Recent development in aluminium alloys for aerospace applications, Mater. Sci. Eng. A. 280 (2000) 102–107.
[3] H.X. Li, V.S. Rudnev, X.H. Zheng, T.P. Yarovaya, R.G. Song, Characterization of Al_2O_3 ceramic coatings on 6063 aluminum alloy prepared in borate electrolytes by micro-arc oxidation, J. Alloys Compd. 462 (2008) 99–102.
[4] S. Ji, Y. Weng, Z. Wu, Z. Ma, X. Tian, R.K.Y. Fu, H. Lin, G. Wu, P.K. Chu, F. Pan, Excellent corrosion resistance of P and Fe modified micro-arc oxidation coating on Al alloy, J. Alloys Compd. 710 (2017) 452–459.
[5] P. Wang, T. Wu, Y.T. Xiao, J. Pu, X.Y. Guo, Effects of $Ce(SO_4)_2$ concentration on the properties of micro-arc oxidation coatings on ZL108 aluminum alloys, Mater. Lett. 182 (2016) 27–31.
[6] K.L. Maki, J.M. Hoenig, J.E. Olney, The research progress of micro-arc oxidation on Al and Mg alloys, Mater. Sci. Technol. 14 (2006) 366–369.
[7] J.L. Xu, F. Liu, F.P. Wang, L.C. Zhao, Alumina coating formed on medical NiTi alloy by micro-arc oxidation, Mater. Lett. 62 (2008) 4112–4114.
[8] S.G. Xin, L.X. Song, R.G. Zhao, X.F. Hu, Microstructure and adhesion strength of Al-Si-O micro-arc oxidation coating, J. Inorg. Mater. 21 (2006) 493–498.
[9] T. Wei, F. Yan, J. Tian, Characterization and wear- and corrosion-resistance of microarc oxidation ceramic coatings on aluminum alloy, J. Alloys Compd. 389 (2005) 169–176.
[10] Z. Wang, L. Wu, W. Cai, A. Shan, Z. Jiang, Effects of fluoride on the structure and properties of microarc oxidation coating on aluminium alloy, J. Alloys Compd. 505 (2010) 188–193.
[11] G. Yang, L. Xianyi, Y. Bai, H. Cui, Z. Jin, The effects of current density on the phase composition and microstructure properties of micro-arc oxidation coating, J. Alloys Compd. 345 (2002) 196–200.
[12] A.L. Yerokhin, A. Shatrov, V. Samsonov, P. Shashkov, A. Leyland, A. Matthews, Fatigue properties of Keronite® coatings on a magnesium alloy, Surf. Coating. Technol. 182 (2004) 78–84.
[13] A. Leoni, I. Apachitei, A.C. Riemslag, L.E. Fratila-Apachitei, J. Duszczyk, In vitro fatigue behavior of surface oxidized Ti35Zr10Nb biomedical alloy, Mater. Sci. Eng. C 31 (2011) 1779–1783.
[14] K.O.N.G. Dejun, L.I.U. Hao, W.A.N.G. Jinchun, Effects of micro arc oxidation on fatigue limits and fracture morphologies of 7475 high strength aluminum alloy, J. Alloys Compd. 650 (2015) 393–398.
[15] B. Lonyuk, I. Apachitei, J. Duszczyk, The effect of oxide coatings on fatigue properties of 7475-T6 aluminium alloy, Surf. Coating. Technol. 201 (2007) 8688–8694.
[16] Y.M. Wang, P.F. Zhang, L.X. Guo, J.H. Ouyang, Y. Zhou, D.C. Jia, Effect of microarc oxidation coating on fatigue performance of Ti-Al-Zr alloy, Appl. Surf. Sci. 255 (2009) 8616–8623.
[17] D.T. Asquith, A.L. Yerokhin, J.R. Yates, A. Matthews, Effect of combined shot-peening and PEO treatment on fatigue life of 2024Al alloy, Thin Solid Films 515 (2006) 1187–1191.
[18] W. Lei, Y. Wang, Y. Jin, D. Sun, Design and characterization of SMAT-MAO composite coating and its influence on the fatigue property of 2024 Al alloy, Rare Metal Mater. Eng. 43 (2014) 1582–1587.
[19] X.S. Wang, X.W. Guo, X.D. Li, D.Y. Ge, Improvement on the fatigue performance of 2024-T4 alloy by synergistic coating technology, Materials 7 (2014) 3533–3546.
[20] H. Tang, F. Wang, Synthesis and properties of CaTiO3-containing coating on AZ31 magnesium alloy by micro-arc oxidation, Mater. Lett. 93 (2013) 427–430.
[21] T. Arunnellaiappan, N.K. Babu, L.R. Krishna, N. Rameshbabu, Influence of frequency and duty cycle on microstructure of plasma electrolytic oxidized AA7075 and the correlation to its corrosion behavior, Surf. Coating. Technol. 280 (2015) 136–147.
[22] J.M. Yang, Y.C. Her, N. Han, A. Clauer, Laser shock peening on fatigue behavior of 2024-T3 Al alloy with fastener holes and stopholes, Mater. Sci. Eng. A. 298 (2001) 296–299.
[23] W. Xue, Z. Deng, R. Chen, T. Zhang, Growth regularity of ceramic coatings formed by microarc oxidation on Al–Cu–Mg alloy, Thin Solid Films 372 (2000) 114–117.
[24] W.-C. Gu, G.-H. Lv, H. Chen, G.-L. Chen, W.-R. Feng, S.-Z. Yang, Characterisation of ceramic coatings produced by plasma electrolytic oxidation of aluminum alloy, Mater. Sci. Eng. A. 447 (2007) 158–162.
[25] M.C. Dourado, F. Protti, J.L. Szwarcfiter, Fatigue behavior and physical characterization of surface-modified Ti-6Al-4V ELI alloy by micro-arc oxidation, Mater. Res. 15 (2012) 305–311.
[26] H.F. Weng, Q.L. Chen, C. Xun, M.D. Bao, Effects of pulse duty cycles on microarc oxidation formed on Al, Surf. Technol. 34 (2005) 59–62.
[27] V. Dehnavi, B.L. Luan, D.W. Shoesmith, X.Y. Liu, S. Rohani, Effect of duty cycle and applied current frequency on plasma electrolytic oxidation (PEO) coating growth behavior, Surf. Coating. Technol. 226 (2013) 100–107.
[28] R.H.U. Khan, A. Yerokhin, X. Li, H. Dong, A. Matthews, Surface characterisation of DC plasma electrolytic oxidation treated 6082 aluminium alloy: effect of current density and electrolyte concentration, Surf. Coating. Technol. 205 (2010) 1679–1688.
[29] N.P. Wasekar, N. Ravi, P. Suresh Babu, L. Rama Krishna, G. Sundararajan, High-cycle fatigue behavior of microarc oxidation coatings deposited on a 6061-T6 Al alloy, Metall. Mater. Trans. A. 41 (2010) 255–265.
[30] I. Apachitei, B. Lonyuk, L.E. Fratila, Fatigue response of porous coated titanium biomedical alloys, Scripta Mater. 61 (2009) 113–116.
[31] K. Minakawa, Fatigue of titanium alloys, Tetsu-To-Hagane 75 (2009) 1104–1111.
[32] C. Li, W. Dai, F. Duan, Y. Zhang, D. He, Fatigue life estimation of medium-carbon steel with different surface roughness, Appl. Sci. 7 (2017) 338.
[33] L.C. CaMPanelli, L.T. Duarte, C. Bolfarini, Fatigue behavior of modified surface of Ti–6Al–7Nb and CP-Ti by micro-arc oxidation, Mater. Des. 64 (2014) 393–399.
[34] C. Li, S. Li, F. Duan, Y. Wang, Y. Zhang, D. He, Z. Li, W. Wang, Statistical analysis and fatigue life estimations for quenched and tempered steel at different tempering temperatures, Met. - Open Access Metall. J. 7 (2017) 312.